

PONTIFÍCIA UNIVERSIDADE CATÓLICA  
DO RIO DE JANEIRO



**Lucas Lira Lopez Rego**

**Fatigue characterization of metal  
alloys using thermography**

**Projeto de Graduação**

Projeto de Graduação presented to Departamento de Engenharia  
Mecânica da PUC-Rio

Advisor: Jaime Tupiassú Pinho de Castro  
Co-advisor: Vitor Eboli Lopes Paiva

Rio de Janeiro  
December 2017

To Lolita, Manoel, Emerita, Maydée, Flavio and  
Irene. I promise to keep honoring who I am.

## EPIGRAPH

“Educate the children and it won’t be necessary  
to punish the men”.

Pythagoras

## **ACKNOWLEDGMENTS**

I'm very grateful to my advisor, professor Jaime Tupiassú Pinho de Castro in this work and other related ones, for the opportunity and confidence to develop such project. Thanks to him I was able to show my effort and achieve great personal achievements.

I also want to thank professor José Luiz de França Freire, besides sharing this new technique, your lessons have given me great learning.

I have to thank Vitor for teaching me many practical things in the laboratory daily basis, and also sharing your experience and advice.

I would like to thank Marco, Julián and Adrian, for all laboratory support given to me.

Finally I want to thank my family and friends, for helping me indirectly in this journey, they are the most valuable thing I have.

## **ABSTRACT**

### **Fatigue characterization of metal alloys using thermography**

Even though the use of thermography as a non-destructive testing method is relatively well known, its use as a reliable tool for measuring the fatigue properties of metals is not. However, analyzing the temperature rise on the external surface of a structural component during cyclic loading can provide a reliable measure of its fatigue limit, avoiding the need for destructive tests and requiring much less time than standard test methods. It's also possible to determine the SN curve and the influence of the mean stress on its behavior through the same methodology, correlating an energy parameter with the assumption of its dependency on the stress amplitude. For the accomplishment of this work two metallic alloys were chosen, the C36000 brass alloy and 6351-T6 aluminium alloy. The results presented here show good agreement between the predicted and measured fatigue limits and mean stress influenced SN curves.

Keywords: IR Thermography, Fatigue, Thermographic Method, Fatigue Limit, Fatigue curve.

## **RESUMO**

### **Caracterização à fadiga de ligas metálicas por termografia**

Embora o uso da termografia como um método de teste não destrutivo seja relativamente conhecido, seu uso como ferramenta confiável para medir as propriedades de fadiga dos metais não é. No entanto, a análise do aumento de temperatura na superfície externa de um componente estrutural durante o carregamento cíclico pode fornecer uma medida confiável do seu limite de fadiga, evitando a necessidade de testes destrutivos e exigindo muito menos tempo do que os métodos de teste padrão. Também é possível determinar a curva SN e a influência da tensão média em seu comportamento através da mesma metodologia, correlacionando um parâmetro de energia com a suposição de sua dependência na amplitude de tensão. Para a realização deste trabalho foram escolhidas duas ligas metálicas, a C36000 liga de latão e 6351-T6 liga de alumínio. Os resultados apresentados aqui mostram boa concordância entre os limites de fadiga previstos e medidos e as curvas SN influenciadas pela tensão média.

Palavras chaves: Termografia Infravermelha, Fadiga, Método Termográfico, Limite de Fadiga, Curva de Fadiga.

# CONTENTS

1 INTRODUCTION	10
2 IR THERMOGRAPHY METHOD	12
3 MATERIAL AND EXPERIMENTAL PROCEDURE	17
3.1 C36000 COPPER ALLOY	17
3.2 6351-T6 ALUMINIUM ALLOY	18
4 RESULTS AND DISCUSSION	22
5 CONCLUSION	30
REFERENCES	31
APPENDIX A	33
APPENDIX B	41
APPENDIX C	43

## List of figures

2.1 Phases of the thermal behavior of $\Delta T$ vs. N curve for a hot spot in the specimen surface during typical fatigue tests, adapted from (Fargione et al., 2002).	13
2.2 $\Delta T$ vs. N curve for various stress amplitudes $\Delta\sigma_i$ , with the determination of each $\Delta T$	14
2.3 $\Delta T_i$ vs. $\Delta\sigma_i$ curve for various incremental load steps.	14
2.4 Stepped loading procedure for the determination of the fatigue limit and the integral $\phi$ .	16
3.1 Brass specimen tested.	17
3.2 Graphic obtained by the tensile test, adapted from (Nóbrega, 2010).	18
3.3 Aluminium specimen tested, after painted.	18
3.4 INSTRON servo-hydraulic machine during the test.	20
3.5 Camera FLIR A655sc.	20
3.6 Reference and specimen areas and thermal profile used to measure the specimen surface temperature in the fatigue tests.	21
4.1 Average temperature variation measured during a test.	23
4.2 Intersecting lines showing the fatigue limit for C36000 copper alloy test 2 (R= -1).	23
4.3 Fatigue limit evaluation of the seven TS of C36000 copper alloy	26
4.4 Fatigue limit evaluation of the ten TS of 6351-T6 Aluminium alloy.	26
4.5 C36000 graphic alternate stress vs. mean stress for Gerber, Goodman and thermographic.	27
4.6 6351-T6 graphic alternate stress vs. mean stress for Gerber, Goodman and thermographic.	28
4.7 C36000 Fatigue curve for each stress ratio.	29
4.8 6351-T6 Fatigue curve for each stress ratio.	29

## List of tables

3.1 Chemical analysis according to ASTM E30 and ASTM E663, see (Nóbrega, 2010).	17
3.2 Measured mechanical properties for C36000 copper alloy.	17
3.3 Tested Al chemical composition , see (Matweb, 2017).	19
3.4 Measured mechanical properties for 6351-T6 aluminium alloy.	19
4.1 Measured results for each specimen of C36000 copper alloy.	24
4.2 C36000 copper alloy average fatigue limit for each tested R.	24
4.3 Measured results for each specimen of 6351-T6 aluminium alloy.	25
4.4 6351-T6 aluminium alloy average fatigue limit for each tested.	25

## 1 Introduction

Reliable fatigue properties are almost indispensable when designing structural components for long operational lives, as usual in many if not most practical applications. However, measurements of such an important data are so laborious that rarely, if ever, fatigue limits and fatigue curves are properly measured by design engineers in practice. Traditional methodologies, like Dixon's up-and down sequential method and Prot's incremental steps method need to test many fatigue specimens that do not break after lives longer than the lives estimated for the fatigue limits (Castro and Meggiolaro, 2016). Therefore, even for steels, for which fatigue limits can be associated to lives in the order of  $10^6$ - $10^7$  cycles, but especially for many non-ferrous alloys, for which they can be as long as  $5 \cdot 10^8$  cycles, the measurement of fatigue properties by traditional tests are expensive and always take a long time. Analogously, the conventional approach to determine fatigue curves requires a series of tests under different stresses levels with many replications, due to the relatively high dispersion of fatigue crack initiation data. Using this conventional approach, a life span of fatigue for each stress level can be estimated to produce a group of SN curves with varying levels of probability. Due to these difficulties, it is probably a truism to affirm that most long life designs use estimated instead of properly measured fatigue data, even for steel components, which tend to reach fatigue limits at relatively short lives.

However, such laborious traditional tests are not the only way to reliably measure fatigue properties. Indeed, since fatigue failures are associated to a transition from a conservative and non-damaging state to a dissipative and damaging one under cyclic loads, it can be expected that this transition can be associated to an increase in temperature at the location where a fatigue crack is in the process of being initiated. That is the basis for the thermographic method, which uses a suitable thermal camera to measure small temperature increments on the surface of fatigue specimens loaded under a series of incremental constant amplitude load steps, to identify the transition from the

non-damaging state, below the fatigue limit, to the damage accumulation state above it. A methodology to perform such measurements has been recently proposed and tested (Fargione *et al.*, 2002; Freire *et al.*, 2015; La Rosa and Risitano, 1999; Vieira, 2016; Rego *et al.*, 2017; Bandeira *et al.*, 2017), and it is used here to characterize the fatigue properties of a C36000 Cu alloy (commercially known as Free-Cutting brass), commonly used in deep drawn structural components, and a 6351-T6 Al alloy.

The thermographic method reduces the testing costs by decreasing the quantity of required specimens, but it is especially useful because it significantly decreases the testing time. Although realistic measurements of the fatigue limit are often obtained, this approach may still generate questionable results, in particular if used without the necessary precautions. Fatigue limits reported in literature using thermography analyses show variations up to ~20% when compared with Dixon's up-and-down method, depending on the material, equipment and testing conditions, (Cura *et al.*, 2005), but the variations may be much smaller (Bandeira *et al.*, 2017).

## 2 IR Thermography Method

The IR thermography is a technique that allows the thermal mapping of the surface of a body or a region through the use of a sensible thermal camera, with the intention of distinguishing areas with different temperatures, in particular the small ones. It is, therefore, a technique that allows artificial visualization of light within the infrared spectrum. It is within the group of techniques known as nondestructive (NDT), real-time and non-contact.

The methodology proposed by La Rosa and Risitano (1999), which is also known as Risitano Rapid Method (RRM), states that it is possible to evaluate the dynamic behavior of the component and to determine the fatigue limit of the material by analyzing the external surface temperature of suitable specimens during cyclic loading. This method does not need any particular testing machine and obtains reliable results using a limited number of specimens in a very short time, because it can detect incipient fatigue damage without needing to break the fatigue specimens.

When the specimen is loaded below the fatigue limit, its temperature varies very slightly due to the thermoelastic effect, but for stress amplitudes above the fatigue limit the temperature variations are significant. The temperature increments ( $\Delta T$ ) behavior has three phases. They increase during the first part of the test (phase 1), then remain stable for a while (phase 2), and finally rapidly increase prior to failure at a life of  $N_f$  cycles (phase 3), as shown in Fig. 2.1.

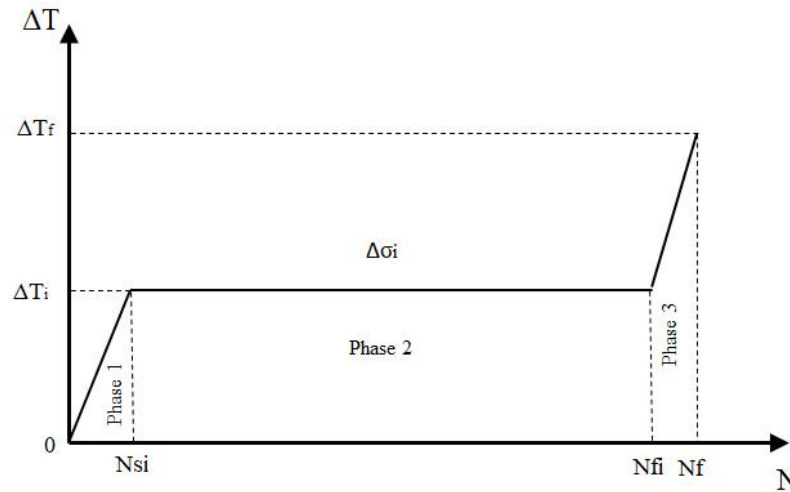


Figure 2.1: Phases of the thermal behavior of  $\Delta T$  vs.  $N$  curve for a hot spot in the specimen surface during typical fatigue tests, adapted from (Fargione *et al.*, 2002).

Through the analysis of the temperature response curve under incremental cyclic step loading, see Fig. 2.2 and 2.3, the fatigue limit can be evaluated considering the heating rate ( $\Delta T/\Delta N$ ) or the stabilized temperature increment  $\Delta T_i$  (La Rosa and Risitano, 1999). Each stress amplitude level corresponds to one stabilization temperature. Two linear regression lines are used to approximate the thermal data and to determine graphically the fatigue limit, as depicted in Fig. 2.3. The first line contains the data where the applied stress is below the fatigue limit, and the second line fits the data located above the limit. The fatigue limit is determined by the intersection of these two lines, as shown in Fig. 2.3. For stress amplitudes below the fatigue limit, the small temperature increments  $\Delta T$  are caused by thermoelastic effects, thus they increase only until a steady-state  $\Delta T_i$  is reached without failure (La Rosa and Risitano, 1999).

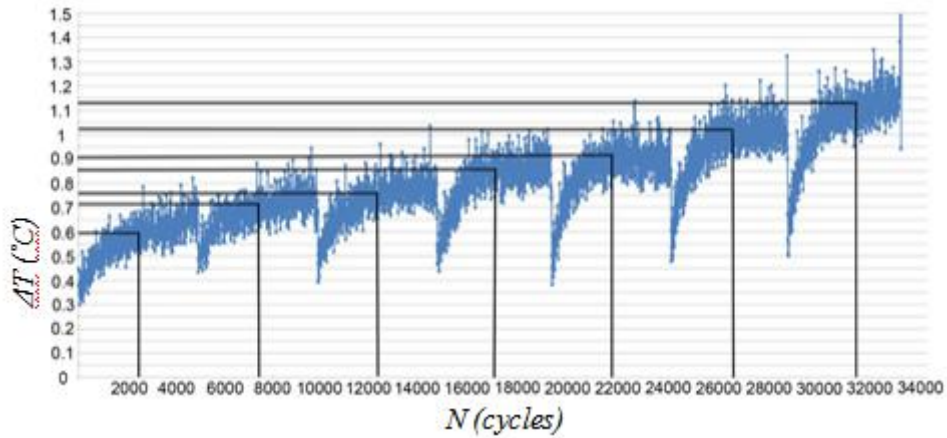


Figure 2.2:  $\Delta T$  vs.  $N$  curve for various stress amplitudes  $\Delta\sigma_i$ , with the determination of each  $\Delta T_i$

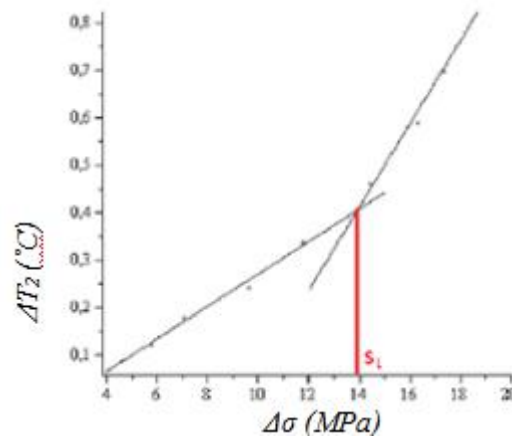


Figure 2.3:  $\Delta T_i$  vs.  $\Delta\sigma_i$  curve for various incremental load steps.

Using the same line of analysis, Fargione *et al.* (2002) proposed a method to determine the fatigue-life curve of the material using IR thermography. This method is much faster than the traditional one and needs theoretically only one specimen. In practice, three is the recommended minimum number of specimens. This method correlates the plastic deformation energy density ( $E_C$ ) with material failure, as seen in Eq. (2-1):

$$E_C = \int_0^{N_f} E_P dN \quad (2-1)$$

where  $E_C$  is the amount of micro-plastic strain energy to failure per unit of volume (a property of the material),  $N_f$  is the number of cycles to failure, and  $E_P$  is the energy due to yielding per unit volume per cycle.

The work done over the system by the loading ( $E_W$ ), as presented in Eq. (2-2), results from the stored internal energy ( $E_i$ ) and the energy converted into heat ( $Q$ ).

$$E_W = E_i + Q \quad (2-2)$$

Assuming  $E_i$  to be small compared to  $Q$ , and using Risitano's results, which have shown  $E_W$  to be proportional to  $Ep$ , Fargione *et al.* (2002) proposed:

$$E_C = \int_0^{T_f} dQ \quad (2-3)$$

For small temperature variations (under 100K, implicating small loading frequencies), the heat transferred from the specimen to the environment can be considered proportional to the temperature difference  $\Delta T$ . Because of that,  $Q$  can be evaluated through a parameter  $\phi$ , which is the integral of the  $\Delta T$  vs.  $N$  curve in Fig. 1, Eq. (2-4):

$$\phi = \int_0^{N_f} \Delta T dN \quad (2-4)$$

In practice,  $\phi$  is assumed constant for given test conditions, such as the specimen geometry and material, loading frequency and environment. This critical value corresponds to fatigue failure and it is associated to the total area under the curve in Fig. 2.1 (for one constant stress amplitude level), or the total dashed area in Fig. 2.4 (for several stress amplitude levels). The  $\phi$  value can be used together with measurements of  $\Delta T_i$ ,  $\Delta T_{oi}$ ,  $\Delta N_i$  at the various stress amplitude levels for a single specimen, as depicted in Fig. 2.4 and modeled by Eq. (2-5) and Eq. (2-6), to yield the whole fatigue SN curve. Each data point of the SN curve is formed by the pair  $(N_{fi}, \Delta\sigma_i)$  where  $N_{fi}$  is calculated from Eq. (2-

5). This equation is derived with the help of Fig.2.4 and the assumption that phase 3 depicted in Fig. 2.1 is small and can be neglected. The value of  $N_{si}$  is determined from Eq. (2-6) with the help of Fig. 2.4.

$$\phi = \Delta T_i \left( N_{fi} - \frac{\Delta N_{si}}{2} \right) \quad (2-5)$$

$$N_{si} = \frac{\Delta N_i \Delta T_i}{\Delta T_i - \Delta T_{0i}} \quad (2-6)$$

The partial damage value  $D_i$  results from the partial integrated value  $\phi_i$  resulting from the application of each stress amplitude  $\Delta\sigma_i$ . The value  $\phi_i$  is calculated considering the number of cycles applied at each stress level,  $N_{pi}$ . The denominator of Eq. (2-7) gives the area under the curve  $\Delta T$  vs.  $N$  considering the interval  $N_{pi}$ . The partial damage value of Eq. (2-7) assumes Miner's linear damage accumulation rule is valid.

$$D_i = \frac{\phi_i}{\phi} = \frac{\left( \frac{\Delta T_i + \Delta T_{0i}}{2} \right) \Delta N_i + \Delta T_i (N_{fi} - \Delta N_{si})}{\sum_1^f \phi_f} \quad (2-7)$$

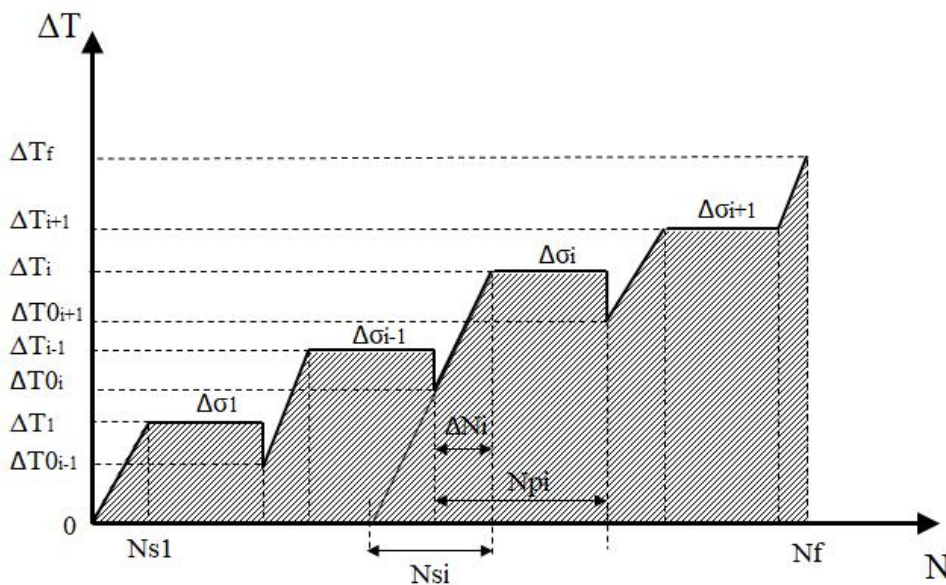


Figure 2.4: Stepped loading procedure for the determination of the fatigue limit and the integral  $\phi$ .

### 3 Material and Experimental Procedure

#### 3.1 C36000 copper alloy

Seven cylindrical specimens made from a C36000 Cu alloy, commercially known as Free-Cutting brass, were tested to evaluate their fatigue behavior using the proposed method. One specimen is presented in Fig. 3.1. The diameter of the uniform gage test section was 10.0 mm, a value verified by the mean of five measurements taken with a micrometer. The chemical composition of this brass was furnished by its supplier, and it is presented in Tab. 3.1, while its basic mechanical properties are shown in Tab. 3.2. These properties were measured in a 100 kN machine with a crosshead speed of 0.9 mm/min according to ASTM E 8M-13a standard (ASTM, 2013) procedures (Nóbrega, 2010).



Figure 3.1: Brass specimen tested.

Element	Cu	Zn	Pb	Fe	Sn	P	Al	Mn
(%)	61,63	35,10	2,92	0,14	0,10	0,010	<0,01	<0,01

Table 3.1: Chemical analysis according to ASTM E30 and ASTM E663, see (Nóbrega, 2010).

Properties	Measured	Obtained from the literature (Nationalbronze, 2017)
Tensile Strength [MPa]	436	450
Rockwell B Hardness	72	70

Table 3.2: Measured mechanical properties for C36000 copper alloy.

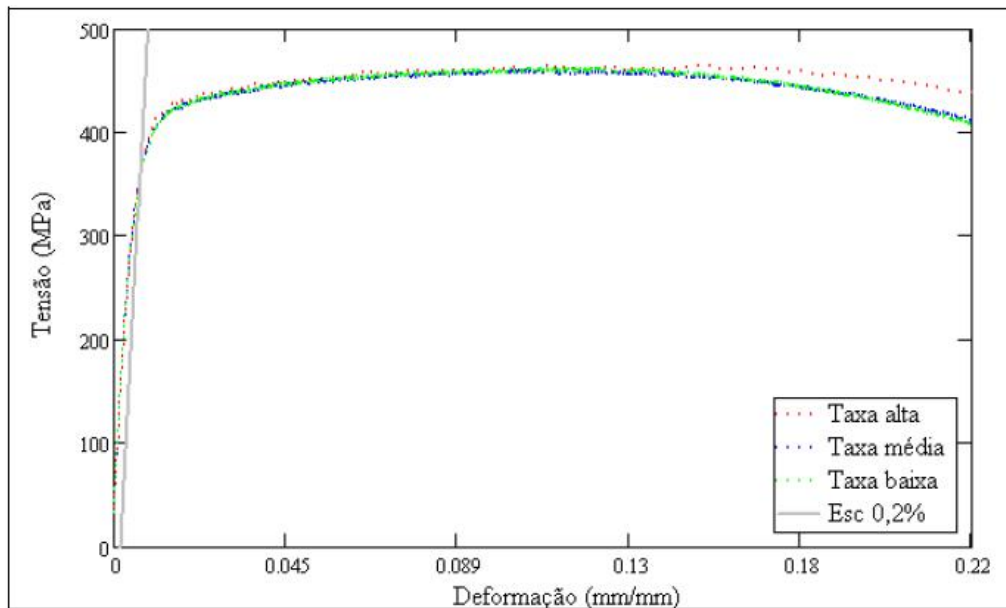


Figure 3.2: Graphic obtained by the tensile test, adapted from (Nóbrega, 2010).

### 3.2 6351-T6 Aluminium alloy

Ten cylindrical specimens made from a 6351-T6 Aluminium alloy, were designed according to ASTM E606 / E606M-12 (ASTM, 2012), they were tested to evaluate their fatigue behavior using the proposed method. One specimen is presented in Fig. 3.3. The diameter of the uniform gage test section was 6.35 mm, a value verified by the mean of five measurements taken with a micrometer. The chemical composition of this Aluminium was obtained through its datasheet, and it is presented in Tab. 3.3, while its basic mechanical properties are shown in Tab. 3.4. These properties were measured in a 100 kN machine with a crosshead speed of 0.9 mm/min according to ASTM E 8M-13a standard (ASTM, 2013) procedures.



Figure 3.3: Aluminium specimen tested, after painted.

Element	Al	Cu	Fe	Mg	Mn	Si	Ti	Zn
(%)	95,9 - 98,5	≤0,10	≤0,50	0,40 - 0,80	0,40 - 0,80	0,70 - 1,3	≤0,20	<0,20

Table 3.3: Tested Al chemical composition , see (Matweb, 2017).

Properties	Measured	Obtained from the literature
Tensile Strength [MPa]	320	310
Vickers Hardness	99	107

Table 3.4: Measured mechanical properties for 6351-T6 aluminium alloy.

The preparation of specimens for thermographic analysis is described by Charles et al. (1975). All specimens were painted with a thin layer of opaque black paint to increase their emissivity, making it close to the value of a black body. The specimens were fatigue tested in a 100 kN INSTRON 8501 servo-hydraulic machine, Fig. 3.4.

During each fatigue test, the surface temperature was recorded in real time by a microbolometer thermocamera FLIR A655sc, see Fig. 3.5. It uses a focal plane array (FPA) of 640×480 pixels, and has spatial resolution of 17 μm, acquisition frequency of 50 Hz on full frame configuration, spectral range from 7.5 to 14 μm, and sensitivity below 30 mK. Temperature data was acquired and analyzed using the ResearchIR software from FLIR. The thermal profile for the first specimen is shown in Fig. 3.6. Environment temperature and heating associated to the loading machine can contribute to increase the surface temperature of specimen (De Finis et al., 2015). In this work, the later factor could be neglected due to the large dimensions of the testing machine and of the grips, the relatively low frequency of the tests, and the low number of cycles for each load step ( $\approx 5 \cdot 10^3$ ). A reference body placed aside the specimen for temperature compensation purposes confirmed the testing system had a negligible effect on the fatigue specimens.

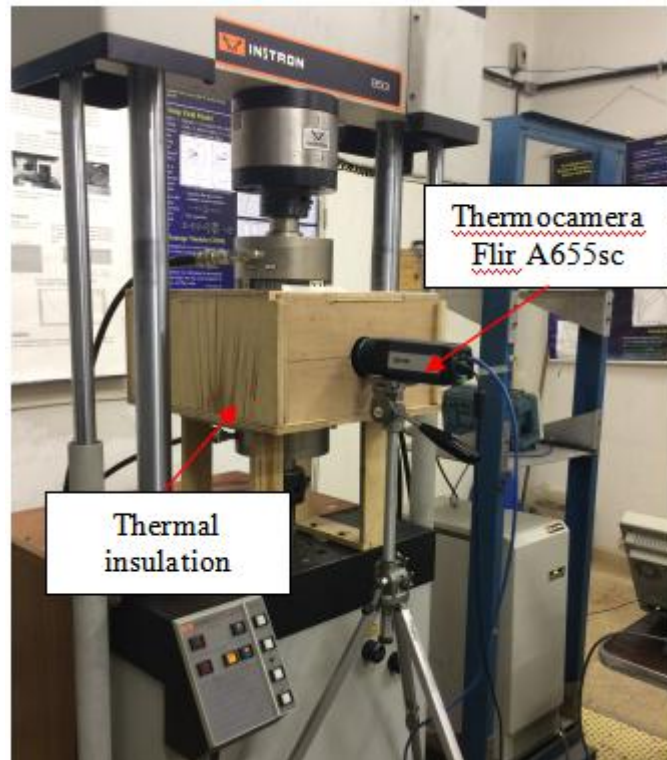


Figure 3.4: INSTRON servo-hydraulic machine during the test.



Figure 3.5: Camera FLIR A655sc.

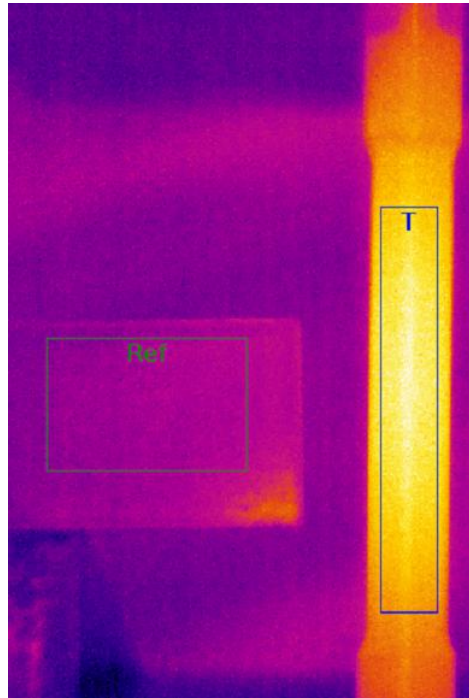


Figure 3.6: Reference and specimen areas and thermal profile used to measure the specimen surface temperature in the fatigue tests.

Based on the experimental methodology proposed by De Finis *et al.* (2015), the specimens were tested under a step loading procedure, sequentially applying to each specimen at a constant amplitude under force-control, with stress ratios  $R = \sigma_{min}/\sigma_{max}$  equal to  $R = -1, 0.5, 0.1$  and  $0.5$ . At each load step, the load amplitude was maintained fixed during blocks of  $5 \cdot 10^3$  cycles, a value that was high enough to achieve a stable thermal behavior, as determined by preliminary tests. Afterwards, the load was increased until the specimen failed.

## 4 Results and Discussion

The temperature variation with number of cycles and applied stress amplitude are presented respectively in Fig. 4.1 and Fig. 4.2. These plots show that the temperature undergoes a significant increase when it is submitted to elevated stress levels, above the fatigue limit. Figure 4.1 shows that temperature stabilizes around 1000 cycles for each stress level, completing the transition from phase 1 to phase 2, as shown in Fig. 2.1. Fig. 4.1 shows that after reaching temperature stabilization, the cyclic loading is kept for approximately 5000 cycles until the test stress level is changed. This way the specimen is consecutively loaded until it finally reaches phase 3 (failure).

Fig. 4.2 shows the stabilized temperatures,  $\Delta T_i$ , obtained from Fig.4.1, plotted against their corresponding amplitude stress levels,  $\Delta\sigma_i$ . According to Ristanos' method, the fatigue limit  $S_L$  can be determined graphically by the intersection of two regression lines based on the data below and above the fatigue limit, as illustrated in Fig. 4.2. When the specimen is subjected to a stress amplitude above the fatigue limit, its temperature increases significantly and damage begins to accumulate in the specimen until the formation of a crack leads it to an eventual failure.

The fatigue limit  $S_L = 139$  MPa determined for C36000 copper alloy specimen 2 under  $R=-1$  determined in Fig. 4.2 and showed in Tab. 4.1 may be compared with typical values listed in Castro and Meggiolaro (2016), for copper alloys from 25% to 50% of their tensile strength, 109 to 218MPa for the tested alloy. The measured fatigue limit is inside this range.

Also the average fatigue limit  $S_L = 134.26$  MPa determined for 6351-T6 aluminium alloy under  $R=-1$  showed in table Tab. 4.4 may be compared with the one calculated by Juvinal's estimation presented in Castro and Meggiolaro (2016), for aluminium alloys with  $S_R \leq 325$ MPa, its fatigue limit is 40% of the tensile strength, 128MPa for the tested alloy.

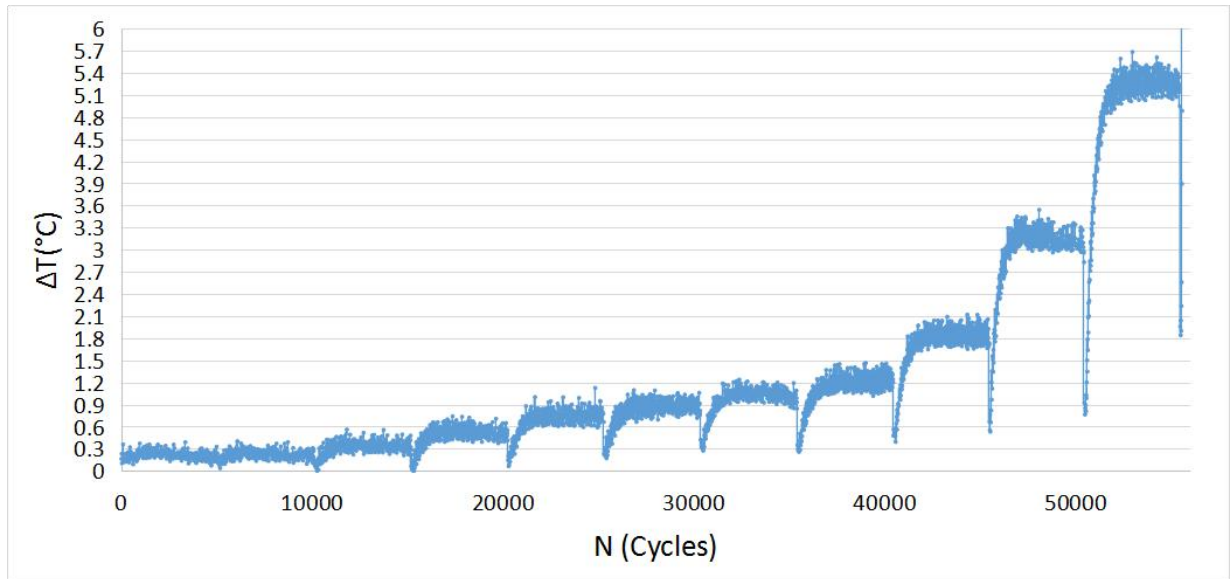


Figure 4.1: Average temperature variation measured during a test.

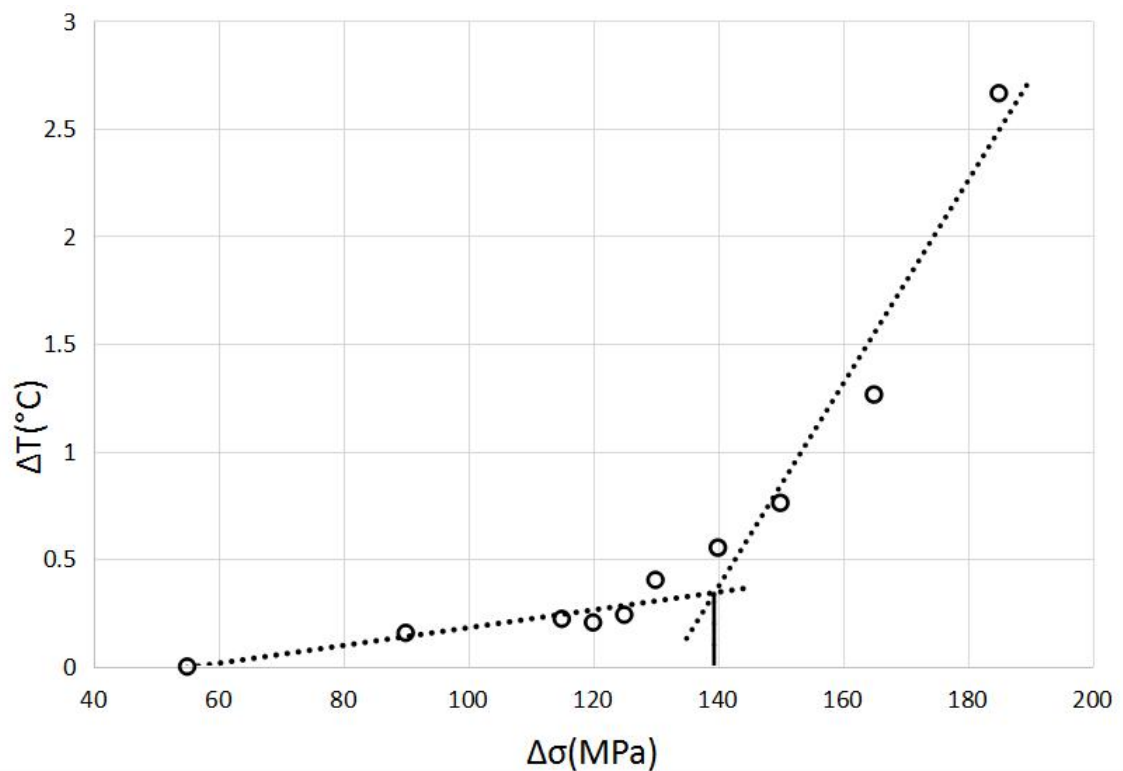


Figure 4.2: Intersecting lines showing the fatigue limit for C36000 copper alloy test 2 ( $R = -1$ ).

Seven specimens of C36000 copper alloy were tested at four different stress ratios ( $R = \sigma_{min}/\sigma_{max}$ ). Test results are summarized in Tab. 4.1 and Tab. 4.2. As shown by Guamán *et al.* (2017), the use of low test frequencies (between 5 and

25Hz) do not affect the measured results. In the present case, three different frequencies were used during the tests (5, 10, and 15Hz). The comparison between the test results using different frequencies shows similar fatigue limits, as it can be seen in Tab. 4.1.

Specimen	Fatigue limit $S_L$ (MPa)	R	Frequency (Hz)	$N_p$ (cycles)	$\phi$ ( $^{\circ}\text{C}\cdot\text{cycles}$ )	$D$ (from Eq. (7))
1*	135.01	-1	15	-	-	-
2	139.39	-1	5	71981	689389.90	0.96
3	122.10	0.1	10	55637	67347.96	0.99
4	119.17	0.1	15	56193	93736.32	0.99
5	131.72	-0.5	15	71550	562041.37	0.97
6	79.95	0.5	15	60975	71292.08	0.99
7	84.21	0.5	15	63337	85012.16	0.94

Table 4.1: Measured results for each specimen of C36000 copper alloy.

\*Specimen 1 was not tested until failure.

$R$	Average Fatigue Limit
-1	137.20
-0.5	131.72
0.1	120.64
0.5	82.08

Table 4.2: C36000 copper alloy average fatigue limit for each tested  $R$ .

Ten specimens of 6351-T6 aluminium alloy were tested at four different stress ratios. Test results are summarized in Tab. 4.3 and Tab. 4.4. In the present case, two different frequencies were used during the tests (15, and 25Hz). The comparison between the test results using different frequencies shows similar fatigue limits, as it can be seen in Tab. 4.3.

Specimen	Fatigue limit SL (MPa)	R	Frequency (Hz)	$N_p$ (cycles)	$\phi$ ( $^{\circ}\text{C}\cdot\text{cycles}$ )	$D$ (from Eq. (7))
1	135.46	-1	15	68344	9096438.41	1
2	132.36	-1	15	73200	15537.47	1
3	104.44	0.1	15	59382	23537.47	0.99
4	115.52	0.1	25	79282	22888.44	0.99
5	125	-0.5	25	121438	27704.13	1
6	134.95	-1	25	113469	26062.67	1
7	105.70	0.1	25	84969	14517.44	1
8	77.26	0.5	25	41957	8409.06	1
9	121.06	-0.5	25	72532	15699.56	1
10	97.43	0.1	25	60469	14149.39	1

Table 4.3: Measured results for each specimen of 6351-T6 aluminium alloy.

$R$	Average Fatigue Limit
-1	134.26
-0.5	123.03
0.1	105.77
0.5	77.26

Table 4.4: 6351-T6 aluminium alloy average fatigue limit for each tested  $R$ .

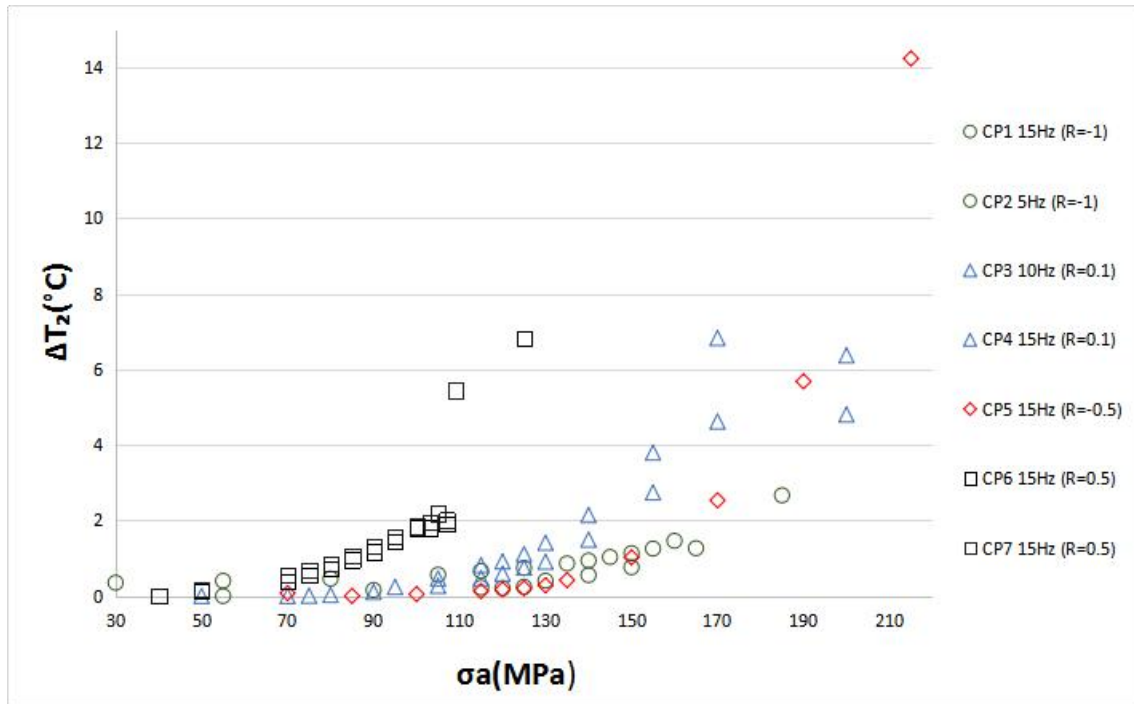


Figure 4.3: Fatigue limit evaluation of the seven TS of C36000 copper alloy.

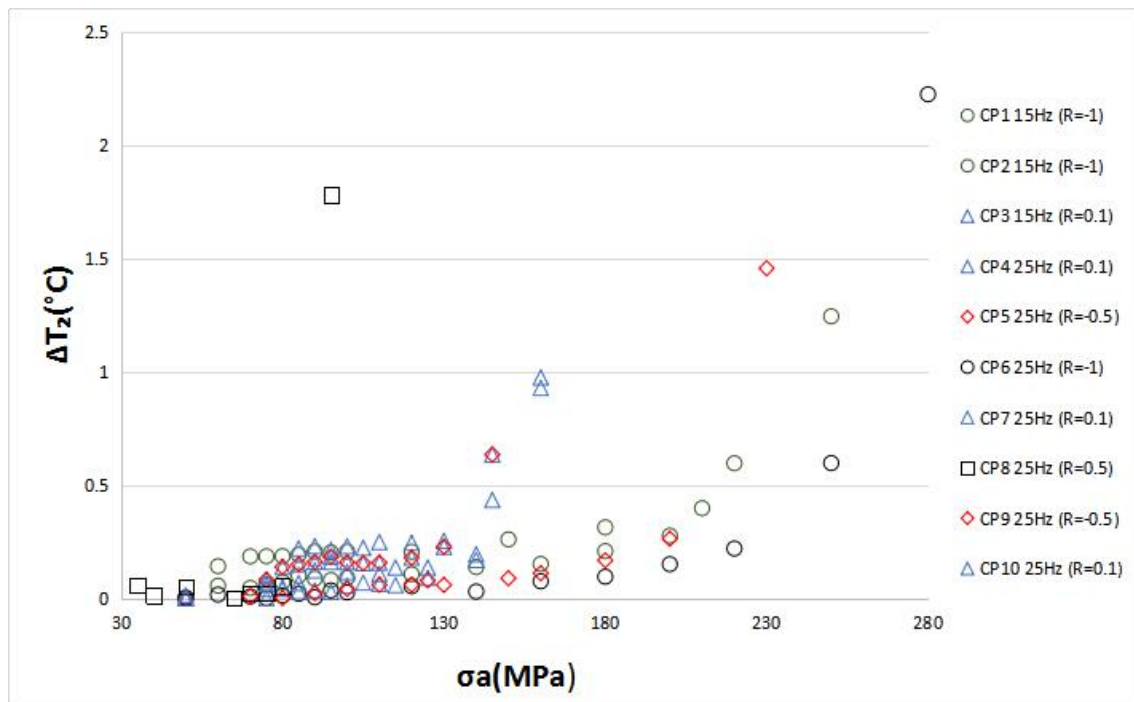


Figure 4.4: Fatigue limit evaluation of the ten TS of 6351-T6 Aluminium alloy.

Based on the average fatigue limit presented in Tab. 4.2 and Tab 4.4 each applied  $R$ , data points formed by pairs of alternate stress amplitude values ( $\sigma_a$ ) and mean stress ( $\sigma_m$ ) were calculated for each material tested and plotted in

Fig. 4.4 and Fig. 4.5. The resulting data was adjusted by a parabolic fitting equation presented in Eq. (4-1), the adjusting exponent  $\alpha$  being equal to 1.65 for C36000 copper alloy and 1.86 for 6351-T6 aluminium alloy. It can be seen that the data of the thermographic tests were well adjusted for the calculated exponent, which is between the exponents given by the so called Goodman and Gerber curves, respectively equal to 1 and 2 (Castro and Meggiolaro, 2016).

$$\frac{\sigma_a}{S_L} + \left( \frac{\sigma_m}{S_u} \right)^\alpha = 1 \quad (4-1)$$

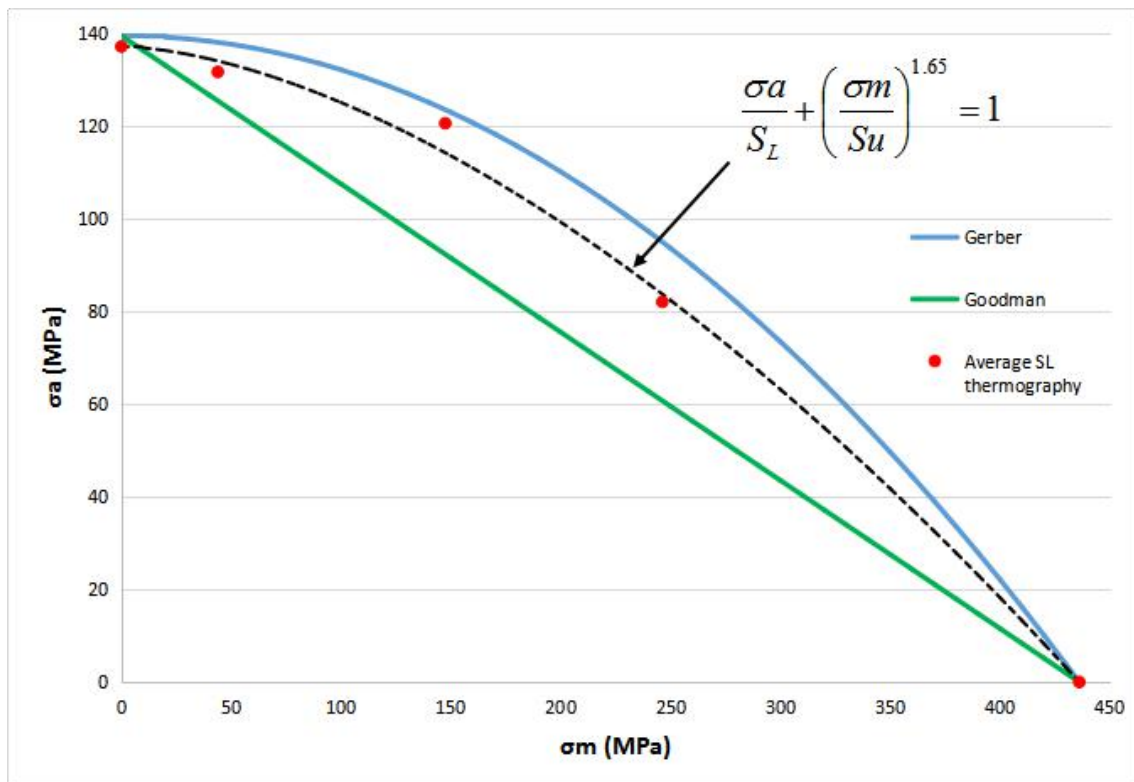


Figure 4.5: C36000 graphic alternate stress vs. mean stress for Gerber, Goodman and thermographic.

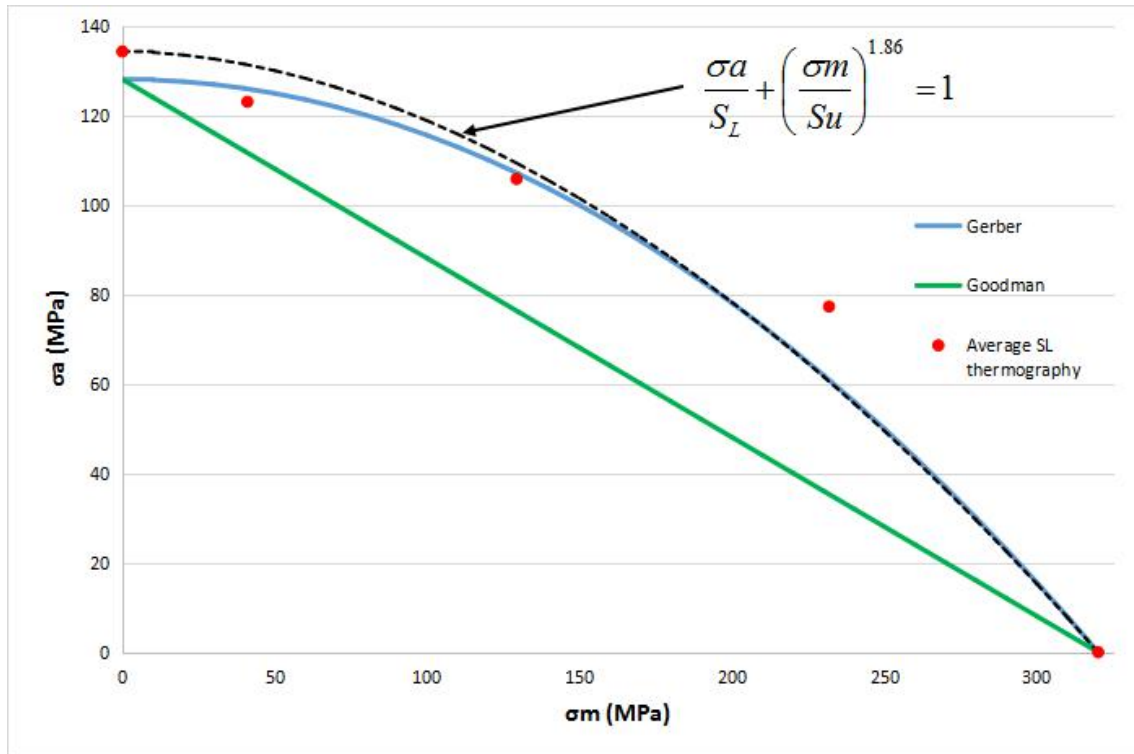


Figure 4.6: 6351-T6 graphic alternate stress vs. mean stress for Gerber, Goodman and thermographic.

Having determined the values of  $\phi$  as presented in Eq. (2-5) and Eq. (2-7), the  $SN$  fatigue curve can be determined using the process outlined in section 2. The  $SN$  fatigue curves for each stress ratio  $R$  calculated in this way for each material tested are presented in Fig. 4.6 and Fig. 4.7. For the C36000 copper alloy the calculated curves encompass data fitted to the interval  $10^4$  to  $10^6$  cycles, also It can be seen that the fatigue curves for  $R = -1$  and  $R = -0.5$  are very similar.

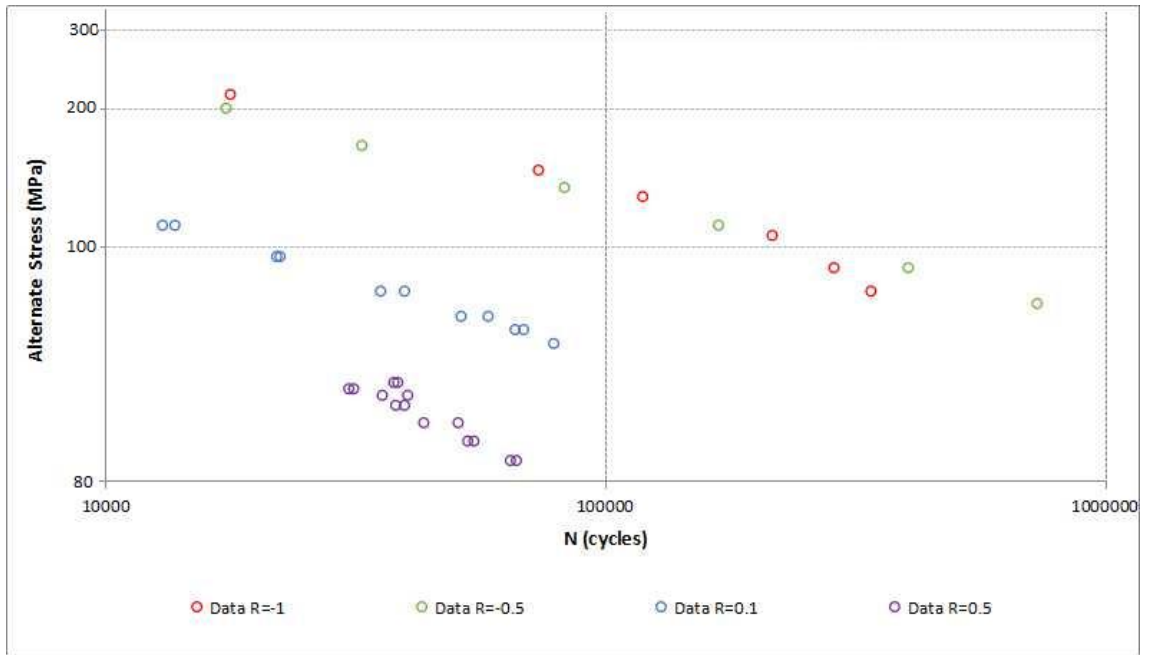


Figure 4.7: C36000 Fatigue curve for each stress ratio.

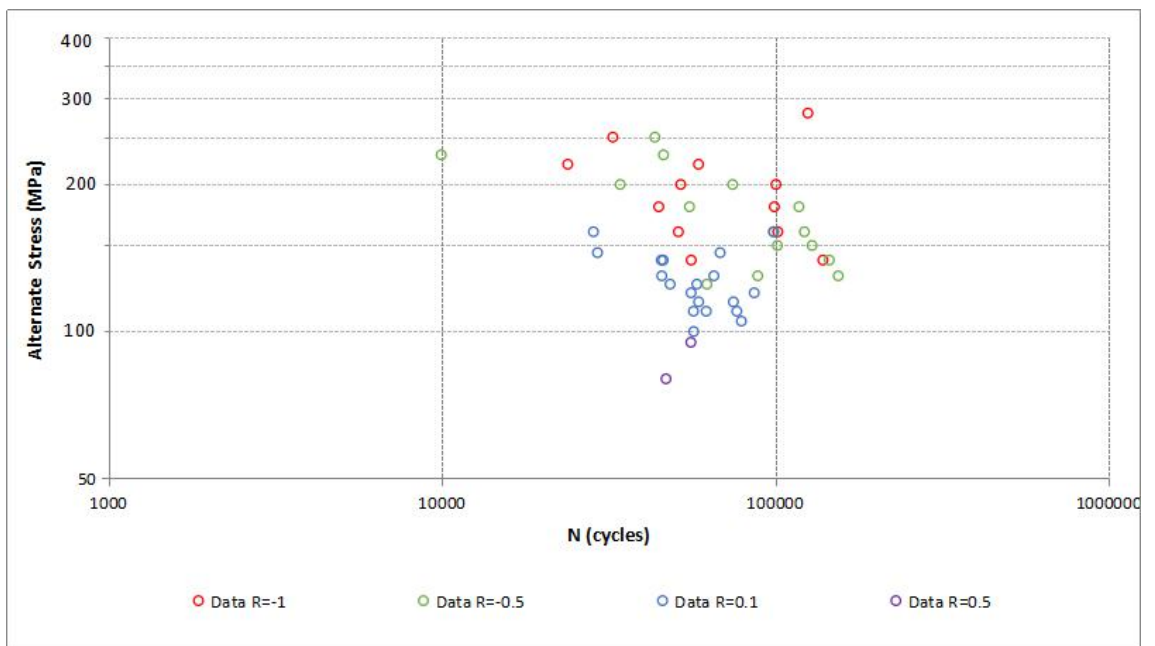


Figure 4.8: 6351-T6 Fatigue curve for each stress ratio.

## 5 CONCLUSION

This work confirms that Risitano's method (La Rosa and Risitano, 1999) is a practical and efficient tool that can provide a reliable and fast way to determine the fatigue behavior of materials using few specimens. More specifically, the work furnishes fatigue data for the C3600 free-cutting brass alloy and 6351-T6 aluminium alloy, which is scarce in the literature. Moreover, the influence of the stress ratio  $R$  was evaluated for this material and an equation showing the influence of the mean applied stress on the fatigue limit was given, which can be useful for design purpose.

With the results and conclusions obtained in this work, the paper entitled: "Fatigue characterization of the C36000 copper alloy using the thermographic method" was presented by the author at the 24<sup>th</sup> ABCM International Congress of Mechanical Engineering, (COBEM 2017). It is shown in the APPENDIX A.

## REFERENCES

- ASTM E 8M–13a, 2013. “Standard Test Methods for Tension Testing of Metallic Materials” *American Society for Testing and Materials*, USA.
- ASTM E606 / E606M-12, Standard Test Method for Strain-Controlled Fatigue Testing, ASTM International, West Conshohocken, PA, 2012.
- Bandeira C. F. C., Kenedi P. P.; Castro J. T. P., Meggiolaro M. A., 2017. "On the use of the thermographic technique to determine the fatigue limit of a cold drawn carbon steel". *Seventh International Conference on Very High Cycle Fatigue*, p.329-334, U. Siegen. ISBN 978-3-00-056960-9.
- Castro J. T. P., Meggiolaro M. A., 2016. “Fatigue Design Techniques, volume 1: High-Cycle Fatigue..” CreateSpace.
- Charles, J.A., Appl, F.J., Francis, J.E., 1975. “Using the scanning infrared camera in experimental fatigue studies”, *Experimental Mechanics*, Vol. 15, p. 133–138.
- Cura, F., Curti, G., Sesana, R., 2005. “A new iteration method for the thermographic determination of fatigue limit in steels”, *International Journal of Fatigue*, Vol. 27, p. 453–459.
- De Finis, R., Palumbo, D., Ancona, F. and Galietti U., 2015., “Fatigue limit evaluation of various martensitic stainless steels with new robust thermographic data analysis”, *International Journal of Fatigue*, Vol.74, p. 88–96.
- Fargione G, Gerarci A, La Rosa G, Risitano A, 2002. Rapid determination of the fatigue curve by the thermographic method. *International Journal of Fatigue*, Vol. 24, p. 11-19.
- Freire J. L. F., Waugh R. C., Fruehmann, R., Dulieu-Barton J. M., 2015. Using thermoelastic stress analysis to detect damaged and hot spot areas in structural components. *J. Mech. Eng. Autom*, Vol. 5, p. 623-634.
- Guamán A., Castro J. T. P., Vieira R. B., Paiva V. E. L., Freire J. L. F., 2017. “Fatigue Limit Assessment of a Low Carbon Steel using Dixon's Up-And-Down and Infrared Thermography Methods” *International Conference on Advances in Experimental Mechanics 29th - 31st August 2017*, University of Sheffield, UK.

La Rosa G, Risitano A., 1999. Thermographic methodology for the rapid determination of the fatigue limit of materials and mechanical components. *Int J Fatigue Mater Struct Components* 1999; Vol. 22, p. 65-73 [December].

Matweb

<[http://www.matweb.com/search/datasheet\\_print.aspx?matguid=ca1cf891973c4745b41677780dad6240](http://www.matweb.com/search/datasheet_print.aspx?matguid=ca1cf891973c4745b41677780dad6240)> 2017. (last accessed 04.12).

Nationalbronze <[www.nationalbronze.com/pdfs/C36000.pdf](http://www.nationalbronze.com/pdfs/C36000.pdf)> 2017. (last accessed 29.09).

Nóbrega M. J. R., 2010. “Influência da metodologia de medição das propriedades mecânicas dinâmicas na previsibilidade do comportamento de estruturas sujeitas a impactos elastoplásticos” *PhD Thesis*, Pontifícia Universidade Católica do Rio de Janeiro, Departamento de Engenharia Mecânica.

Vieira R. B., 2016. “Thermography applied to the study of fatigue in polycarbonate”, *MSc. Thesis*, Pontifícia Universidade Católica do Rio de Janeiro, Departamento de Engenharia Mecânica.

## APPENDIX A -



24th COBEM - 2017

24th ABCM International Congress of Mechanical Engineering  
December 3-8, 2017, Curitiba, PR, Brazil

COBEM-2017-1512

## FATIGUE CHARACTERIZATION OF THE C36000 COPPER ALLOY USING THE THERMOGRAPHIC METHOD

Lucas Lira Lopez Rego  
Jaime Tupiassú Pinho de Castro  
José Luiz de França Freire  
Vitor Eboli Lopes Paiva

Mechanical Engineering Department, Pontifical Catholic University of Rio de Janeiro (PUC-Rio), Rua Marquês de São Vicente 225, Rio de Janeiro, RJ 22453-900, Brazil  
lucaslira20@hotmail.com; jtcastro@puc-rio.br; jlfreire@puc-rio.br; vitoreboli@hotmail.com

**Abstract.** Even though the use of thermography as a non-destructive testing method is relatively well known, its use as a reliable tool for measuring the fatigue properties of metals is not. However, analyzing the temperature rise on the external surface of a structural component during cyclic loading can provide a reliable measure of its fatigue limit, avoiding the need for destructive tests and requiring much less time than standard test methods. It's also possible to determine the SN curve and the influence of the mean stress on its behavior through the same methodology, correlating an energy parameter with the assumption of its dependency on the stress amplitude. The results presented here show good agreement between the predicted and measured fatigue limits and mean stress influenced SN curves.

**Keywords:** IR Thermography, Risitano Method, Fatigue Limits, Fatigue curves.

### 1. INTRODUCTION

Reliable fatigue properties are almost indispensable when designing structural components for long operational lives, as usual in many if not most practical applications. However, measurements of such an important data are so laborious that rarely, if ever, fatigue limits and fatigue curves are properly measured by design engineers in practice. Traditional methodologies, like Dixon's up-and down sequential method and Prot's incremental steps method need to test many fatigue specimens that do not break after lives longer than the lives estimated for the fatigue limits (Castro and Meggiolaro, 2016). Therefore, even for steels, for which fatigue limits can be associated to lives in the order of  $10^6$ - $10^7$  cycles, but especially for many non-ferrous alloys, for which they can be as long as  $5 \cdot 10^8$  cycles, the measurement of fatigue properties by traditional tests are expensive and always take a long time. Analogously, the conventional approach to determine fatigue curves requires a series of tests under different stresses levels with many replications, due to the relatively high dispersion of fatigue crack initiation data. Using this conventional approach, a life span of fatigue for each stress level can be estimated to produce a group of SN curves with varying levels of probability. Due to these difficulties, it is probably a truism to affirm that most long life designs use estimated instead of properly measured fatigue data, even for steel components, which tend to reach fatigue limits at relatively short lives.

However, such laborious traditional tests are not the only way to reliably measure fatigue properties. Indeed, since fatigue failures are associated to a transition from a conservative and non-damaging state to a dissipative and damaging one under cyclic loads, it can be expected that this transition can be associated to an increase in temperature at the location where a fatigue crack is in the process of being initiated. That is the basis for the thermographic method, which uses a suitable thermal camera to measure small temperature increments on the surface of fatigue specimens loaded under a series of incremental constant amplitude load steps, to identify the transition from the non-damaging state, below the fatigue limit, to the damage accumulation state above it. A methodology to perform such measurements has been recently proposed and tested (Fargione *et al.*, 2002; Freire *et al.*, 2015; La Rosa and Risitano, 1999; Vieira, 2016; Bandeira *et al.*, 2017), and it is used here to characterize the fatigue properties of a C36000 Cu alloy (commercially known as Free-Cutting brass), commonly used in deep drawn structural components.

The thermographic method reduces the testing costs by decreasing the quantity of required specimens, but it is especially useful because it significantly decreases the testing time. Although realistic measurements of the fatigue limit are often obtained, this approach may still generate questionable results, in particular if used without the necessary precautions. Fatigue limits reported in literature using thermography analyses show variations up to ~20% when

L. L. L. Rego, J. T. P. Castro, J. L. F. Freire and V. E. L. Paiva  
Fatigue characterization of the C36000 copper alloy using the thermographic method

compared with Dixon's up-and-down method, depending on the material, equipment and testing conditions, (Cura *et al.*, 2005), but the variations may be much smaller (Bandeira *et al.*, 2017).

## 2. IR THERMOGRAPHY METHOD

The IR thermography is a technique that allows the thermal mapping of the surface of a body or a region through the use of a sensible thermal camera, with the intention of distinguishing areas with different temperatures, in particular the small ones. It is, therefore, a technique that allows artificial visualization of light within the infrared spectrum. It is within the group of techniques known as nondestructive (NDT), real-time and non-contact.

The methodology proposed by La Rosa and Risitano (1999), which is also known as Risitano Rapid Method (RRM), states that it is possible to evaluate the dynamic behavior of the component and to determine the fatigue limit of the material by analyzing the external surface temperature of suitable specimens during cyclic loading. This method does not need any particular testing machine and obtains reliable results using a limited number of specimens in a very short time, because it can detect incipient fatigue damage without needing to break the fatigue specimens.

When the specimen is loaded below the fatigue limit, its temperature varies very slightly due to the thermoelastic effect, but for stress amplitudes above the fatigue limit the temperature variations are significant. The temperature increments ( $\Delta T$ ) behavior has three phases. They increase during the first part of the test (phase 1), then remain stable for a while (phase 2), and finally rapidly increase prior to failure at a life of  $N_f$  cycles (phase 3), as shown in Fig. 1.

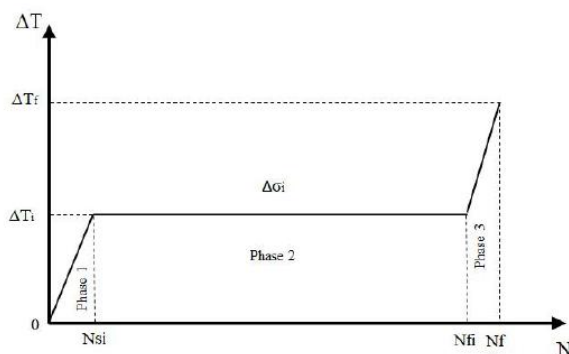


Figure 1: Phases of the thermal behavior of  $\Delta T$  vs.  $N$  curve for a hot spot in the specimen surface during typical fatigue tests, adapted from (Fargione *et al.*, 2002).

Through the analysis of the temperature response curve under incremental cyclic step loading, see Fig. 2A and 2B, the fatigue limit can be evaluated considering the heating rate ( $\Delta T/\Delta N$ ) or the stabilized temperature increment  $\Delta T_i$  (La Rosa and Risitano, 1999). Each stress amplitude level corresponds to one stabilization temperature. Two linear regression lines are used to approximate the thermal data and to determine graphically the fatigue limit, as depicted in Fig. 2B. The first line contains the data where the applied stress is below the fatigue limit, and the second line fits the data located above the limit. The fatigue limit is determined by the intersection of these two lines, as shown in Fig. 2B. For stress amplitudes below the fatigue limit, the small temperature increments  $\Delta T$  are caused by thermoelastic effects, thus they increase only until a steady-state  $\Delta T_i$  is reached without failure (La Rosa and Risitano, 1999).

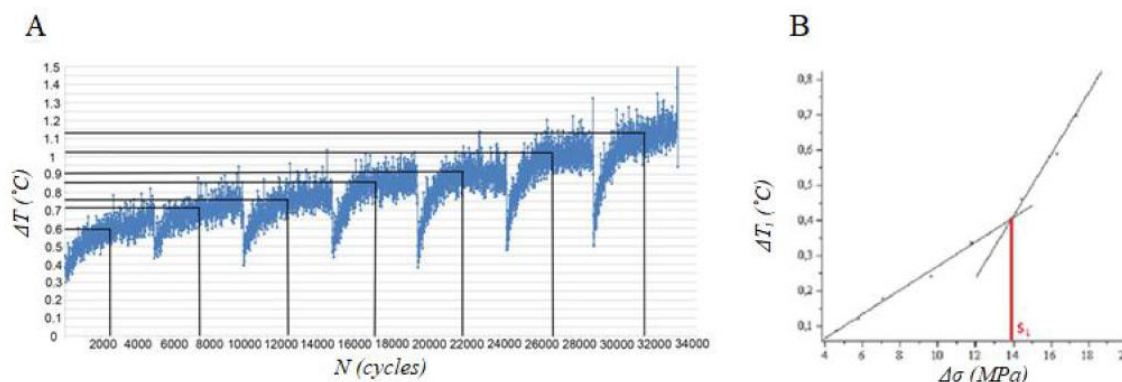


Figure 2: A)  $\Delta T$  vs.  $N$  curve for various stress amplitudes  $\Delta \sigma_i$ , with the determination of each  $\Delta T_i$ ; B)  $\Delta T_i$  vs.  $\Delta \sigma_i$  curve for various incremental load steps.

Using the same line of analysis, Fargione *et al.* (2002) proposed a method to determine the fatigue-life curve of the material using IR thermography. This method is much faster than the traditional one and needs theoretically only one specimen. In practice, three is the recommended minimum number of specimens. This method correlates the plastic deformation energy density ( $E_C$ ) with material failure, as seen in Eq. (1):

$$E_C = \int_0^{N_f} E_p dN \quad (1)$$

where  $E_C$  is the amount of micro-plastic strain energy to failure per unit of volume (a property of the material),  $N_f$  is the number of cycles to failure, and  $E_p$  is the energy due to yielding per unit volume per cycle.

The work done over the system by the loading ( $E_w$ ), as presented in Eq. (2), results from the stored internal energy ( $E_i$ ) and the energy converted into heat ( $Q$ ).

$$E_w = E_i + Q \quad (2)$$

Assuming  $E_i$  to be small compared to  $Q$ , and using Risitano's results, which have shown  $E_w$  to be proportional to  $E_p$ , Fargione *et al.* (2002) proposed:

$$E_C = \int_0^{T_f} dQ \quad (3)$$

For small temperature variations (under 100K, implicating small loading frequencies), the heat transferred from the specimen to the environment can be considered proportional to the temperature difference  $\Delta T$ . Because of that,  $Q$  can be evaluated through a parameter  $\phi$ , which is the integral of the  $\Delta T$  vs.  $N$  curve in Fig. 1, Eq. (4):

$$\phi = \int_0^{N_f} \Delta T dN \quad (4)$$

In practice,  $\phi$  is assumed constant for given test conditions, such as the specimen geometry and material, loading frequency and environment. This critical value corresponds to fatigue failure and it is associated to the total area under the curve in Fig. 1 (for one constant stress amplitude level), or the total dashed area in Fig.3 (for several stress amplitude levels). The  $\phi$  value can be used together with measurements of  $\Delta T_i$ ,  $\Delta T_{0i}$ ,  $\Delta N_i$  at the various stress amplitude levels for a single specimen, as depicted in Fig. 3 and modeled by Eq. (5) and Eq. (6), to yield the whole fatigue SN curve. Each data point of the SN curve is formed by the pair  $(N_{fi}, \Delta\sigma_i)$  where  $N_{fi}$  is calculated from Eq. (5). This equation is derived with the help of Fig.3 and the assumption that phase 3 depicted in Fig. 1 is small and can be neglected. The value of  $N_{st}$  is determined from Eq. 6 with the help of Fig. 3.

$$\phi = \Delta T_i \left( N_{fi} - \frac{\Delta N_{st}}{2} \right) \quad (5)$$

$$N_{st} = \frac{\Delta N_i \Delta T_i}{\Delta T_i - \Delta T_{0i}} \quad (6)$$

The partial damage value  $D_i$  results from the partial integrated value  $\phi_i$  resulting from the application of each stress amplitude  $\Delta\sigma_i$ . The value  $\phi_i$  is calculated considering the number of cycles applied at each stress level,  $N_{pi}$ . The denominator of Eq. (7) gives the area under the curve  $\Delta T$  vs.  $N$  considering the interval  $N_{pi}$ . The partial damage value of Eq. (7) assumes Miner's linear damage accumulation rule is valid.

$$D_i = \frac{\phi_i}{\phi} = \frac{\left( \frac{\Delta T_i + \Delta T_{0i}}{2} \right) \Delta N_i + \Delta T_i (N_{fi} - \Delta N_{st})}{\sum_1^f \phi_f} \quad (7)$$

L. L. L. Rego, J. T. P. Castro, J. L. F. Freire and V. E. L. Paiva  
Fatigue characterization of the C36000 copper alloy using the thermographic method

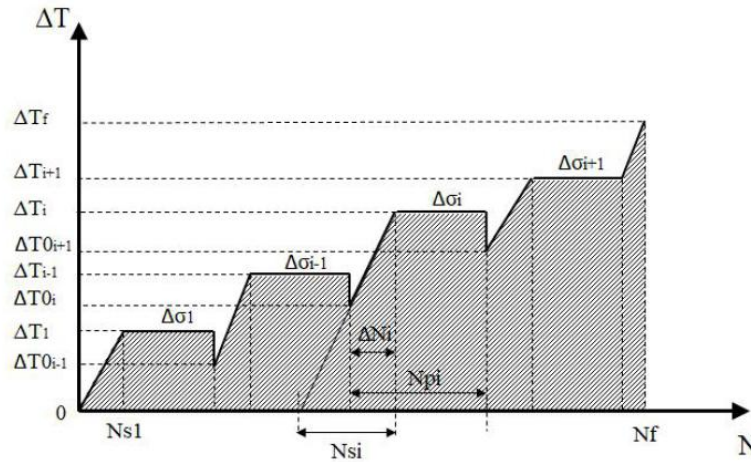


Figure 3: Stepped loading procedure for the determination of the fatigue limit and the integral  $\phi$ .

### 3. MATERIAL AND EXPERIMENTAL PROCEDURE

Seven cylindrical specimens made from a C36000 Cu alloy, commercially known as Free-Cutting brass, were tested to evaluate their fatigue behavior using the proposed method. One specimen is presented in Fig. 4. The diameter of the uniform gage test section was 10.0 mm, a value verified by the mean of five measurements taken with a micrometer. The chemical composition of this brass was furnished by its supplier, and it is presented in Tab. 1, while its basic mechanical properties are shown in Tab. 2. These properties were measured in a 100 kN machine with a crosshead speed of 0.9 mm/min according to ASTM E 8M–13a standard (ASTM, 2013) procedures (Nóbrega, 2010).



Figure 4: Brass specimen tested.

Table 1: Chemical analysis according to ASTM E30 and ASTM E663, see (Nóbrega, 2010).

Element (%)	Cu	Zn	Pb	Fe	Sn	P	Al	Mn
	61.63	35.10	2.92	0.14	0.10	0.010	<0,01	<0,01

Table 2: Measured mechanical properties.

Properties	Measured	Obtained from the literature (Nationalbronze, 2017)
Tensile Strength [MPa]	436	450
Rockwell B Hardness	72	70

The preparation of specimens for thermographic analysis is described by Charles *et al.* (1975). All specimens were painted with a thin layer of opaque black paint to increase their emissivity, making it close to the value of a black body. The specimens were fatigue tested in a 100 kN INSTRON 8501 servo-hydraulic machine, Fig. 5.

During each fatigue test, the surface temperature was recorded in real time by a microbolometer thermocamera FLIR A655sc, see Fig. 6A. It uses a focal plane array (FPA) of 640×480 pixels, and has spatial resolution of 17  $\mu\text{m}$ , acquisition frequency of 50 Hz on full frame configuration, spectral range from 7.5 to 14  $\mu\text{m}$ , and sensitivity below 30 mK. Temperature data was acquired and analyzed using the ResearchIR software from FLIR. The thermal profile for the first specimen is shown in Fig. 6B. Environment temperature and heating associated to the loading machine can contribute to increase the surface temperature of specimen (De Finis *et al.*, 2015). In this work, the later factor could be neglected due to the large dimensions of the testing machine and of the grips, the relatively low frequency of the tests, and the low number of cycles for each load step ( $\approx 5 \cdot 10^3$ ). A reference body placed aside the specimen for temperature compensation purposes confirmed the testing system had a negligible effect on the fatigue specimens.

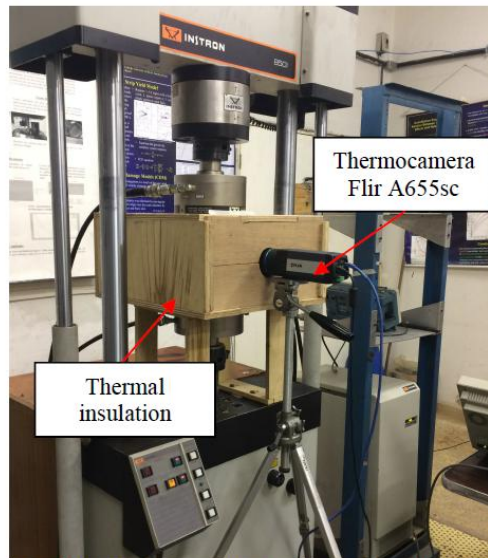


Figure 5: INSTRON servo-hydraulic machine during the test.

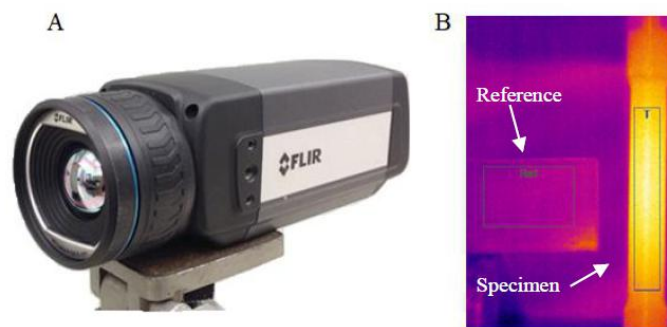


Figure 6: A) Camera FLIR A655sc; B) Reference and specimen areas and thermal profile used to measure the specimen surface temperature in the fatigue tests.

Based on the experimental methodology proposed by De Finis *et al.* (2015), the specimens were tested under a step loading procedure, sequentially applying to each specimen at a constant amplitude under force-control, with stress ratios  $R = \sigma_{min}/\sigma_{max}$  equal to  $R = -1, -0.5, 0.1$  and  $0.5$ . At each load step, the load amplitude was maintained fixed during blocks of  $5 \cdot 10^3$  cycles, a value that was high enough to achieve a stable thermal behavior, as determined by preliminary tests. Afterwards, the load was increased until the specimen failed.

#### 4. RESULTS AND DISCUSSION

The temperature variation with number of cycles and applied stress amplitude are presented respectively in Fig. 7 and Fig. 8. These plots show that the temperature undergoes a significant increase when it is submitted to elevated stress levels, above the fatigue limit. Figure 7 shows that temperature stabilizes around 1000 cycles for each stress level, completing the transition from phase 1 to phase 2, as shown in Fig. 1. Fig. 7 shows that after reaching temperature stabilization, the cyclic loading is kept for approximately 5000 cycles until the test stress level is changed. This way the specimen is consecutively loaded until it finally reaches phase 3 (failure).

Fig. 8 shows the stabilized temperatures,  $\Delta T_i$ , obtained from Fig. 7, plotted against their corresponding amplitude stress levels,  $\Delta \sigma_i$ . According to Ristanos' method, the fatigue limit  $S_L$  can be determined graphically by the intersection of two regression lines based on the data below and above the fatigue limit, as illustrated in Fig. 8. When the specimen is subjected to a stress amplitude above the fatigue limit, its temperature increases significantly and damage begins to accumulate in the specimen until the formation of a crack leads it to an eventual failure. The fatigue limit  $S_L = 139$  MPa determined for specimen 2 under  $R = -1$  determined in Fig. 8 may be compared with typical values listed in Castro and Meggiolaro (2016), for copper alloys from 25% to 50% of their tensile strength, 109 to 218MPa for the tested alloy. The measured fatigue limit is inside this range.

L. L. L. Rego, J. T. P. Castro, J. L. F. Freire and V. E. L. Paiva  
 Fatigue characterization of the C36000 copper alloy using the thermographic method

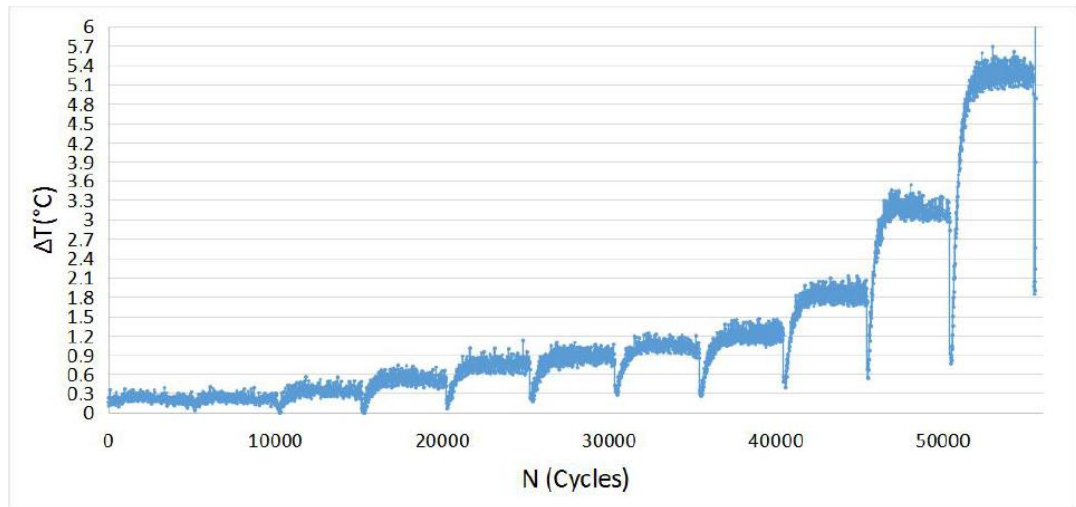


Figure 7: Average temperature variation measured during a test.

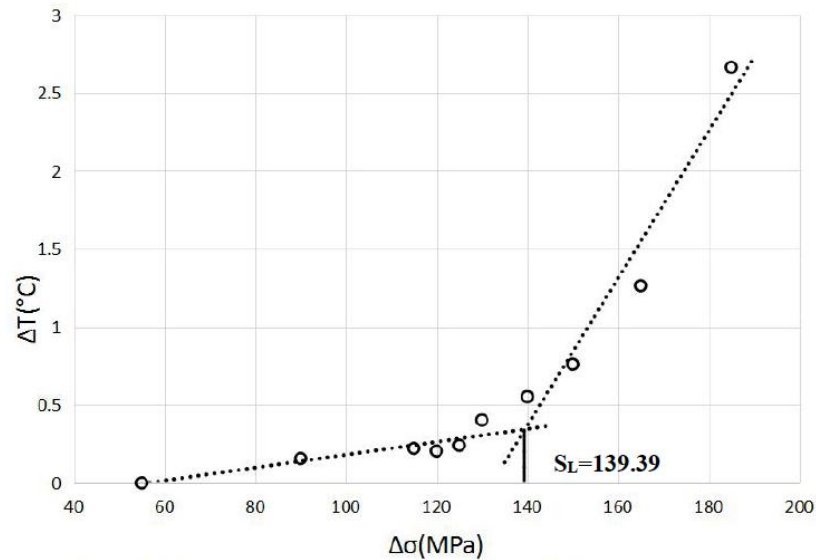


Figure 8: Intersecting lines showing the fatigue limit for test 2 ( $R = -1$ ).

Seven specimens were tested at four different stress ratios ( $R = \sigma_{min}/\sigma_{max}$ ). Test results are summarized in Tab. 3 and Tab. 4. As shown by Guamán *et al.* (2017), the use of low test frequencies (between 5 and 25Hz) do not affect the measured results. In the present case, three different frequencies were used during the tests (5, 10, and 15Hz). The comparison between the test results using different frequencies shows similar fatigue limits, as it can be seen in Tab. 3.

Table 3: Measured results for each specimen.

Specimen	Fatigue limit $S_L$ (MPa)	R	Frequency (Hz)	$N_p$ (cycles)	$\phi$ ( $^{\circ}\text{C}\cdot\text{cycles}$ )	$D$ (from Eq. (7))
1*	135.01	-1	15	-	-	-
2	139.39	-1	5	71981	689389.90	0.96
3	122.10	0.1	10	55637	67347.96	0.99
4	119.17	0.1	15	56193	93736.32	0.99
5	131.72	-0.5	15	71550	562041.37	0.97
6	79.95	0.5	15	60975	71292.08	0.99
7	84.21	0.5	15	63337	85012.16	0.94

\*Specimen 1 was not tested until failure.

Table 4: Average fatigue limit for each tested  $R$ .

$R$	Average Fatigue Limit	Curve Adjusted Fatigue Limit
-1	137.20	138.00
-0.5	131.72	136.50
0.1	120.64	121.89
0.5	82.08	87.72

Based on the average fatigue limit presented in Tab. 4 for each applied  $R$ , data points formed by pairs of alternate stress amplitude values ( $\sigma_a$ ) and mean stresses ( $\sigma_m$ ) were calculated and plotted in Fig. 9. The resulting data was adjusted by a parabolic fitting equation presented in Eq. (8), the adjusting exponent  $\alpha$  being equal to 1.65. It can be seen that the data of the thermographic tests were well adjusted for the calculated exponent, which is between the exponents given by the so called Goodman and Gerber curves, respectively equal to 1 and 2 (Castro and Meggiolaro, 2016).

$$\frac{\sigma_a}{S_L} + \left(\frac{\sigma_m}{S_u}\right)^\alpha = 1 \quad (8)$$

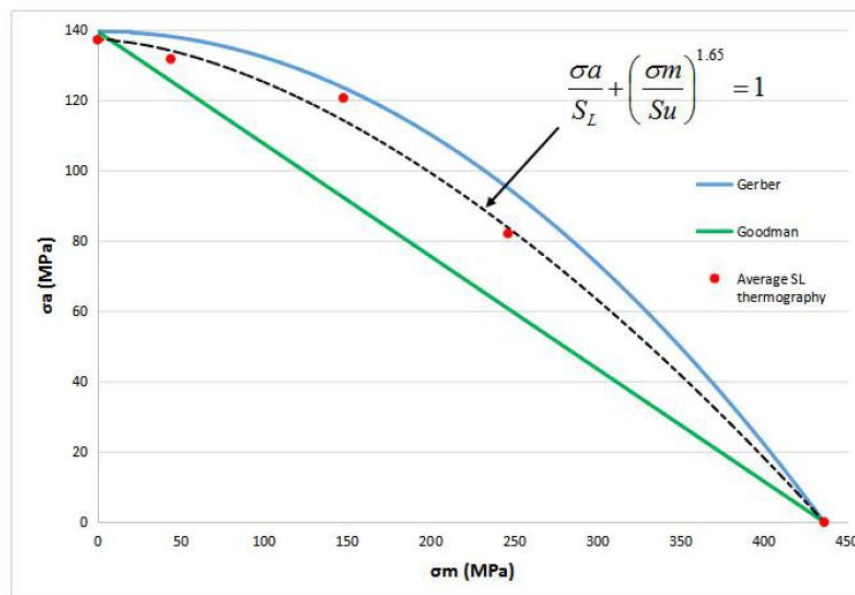


Figure 9: Graphic alternate stress vs. mean stress for Gerber, Goodman and thermographic.

Having determined the values of  $\phi$  as presented in Eq. (5) and Eq. (7), the  $SN$  fatigue curve can be determined using the process outlined in section 2. The  $SN$  fatigue curves for each stress ratio  $R$  calculated in this way are presented in Fig. 10. The calculated curves encompass data fitted to the interval  $10^4$  to  $10^6$  cycles. It can be seen that the fatigue curves for  $R = -1$  and  $R = -0.5$  are very similar.

## 5. CONCLUSIONS

This paper confirms that Risitano's method (La Rosa and Risitano, 1999) is a practical and efficient tool that can provide a reliable and fast way to determine the fatigue behavior of materials using few specimens. More specifically, the paper furnishes fatigue data for the C3600 free-cutting brass alloy, which is scarce in the literature. Moreover, the influence of the stress ratio  $R$  was evaluated for this material and an equation showing the influence of the mean applied stress on the fatigue limit was given, which can be useful for design purpose.

L. L. L. Rego, J. T. P. Castro, J. L. F. Freire and V. E. L. Paiva  
 Fatigue characterization of the C36000 copper alloy using the thermographic method

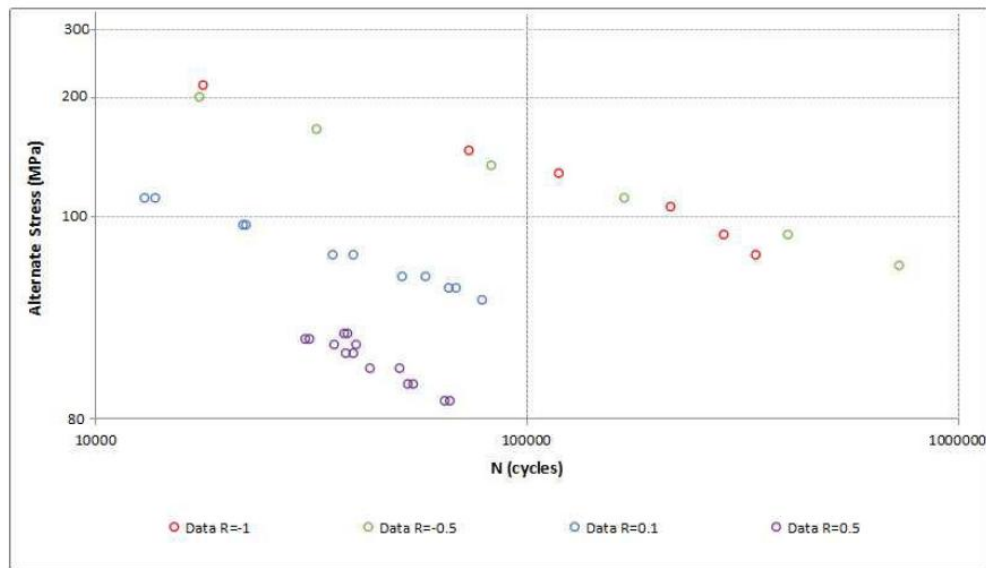


Figure 10: Fatigue curve for each stress ratio.

## 6. REFERENCES

- ASTM E 8M-13a, 2013. "Standard Test Methods for Tension Testing of Metallic Materials" *American Society for Testing and Materials*, USA.
- Bandeira C. F. C., Kenedi P. P.; Castro J. T. P., Meggiolaro M. A., 2017. "On the use of the thermographic technique to determine the fatigue limit of a cold drawn carbon steel". *Seventh International Conference on Very High Cycle Fatigue*, p.329-334, U. Siegen. ISBN 978-3-00-056960-9.
- Castro J. T. P., Meggiolaro M. A., 2016. "Fatigue Design Techniques, volume 1: High-Cycle Fatigue.." CreateSpace.
- Charles, J.A., Appl, F.J., Francis, J.E., 1975. "Using the scanning infrared camera in experimental fatigue studies", *Experimental Mechanics*, Vol. 15, p. 133-138.
- Cura, F., Curti, G., Sesana, R., 2005. "A new iteration method for the thermographic determination of fatigue limit in steels", *International Journal of Fatigue*, Vol. 27, p. 453-459.
- De Finis, R., Palumbo, D., Ancona, F. and Galietti U., 2015., "Fatigue limit evaluation of various martensitic stainless steels with new robust thermographic data analysis", *International Journal of Fatigue*, Vol.74, p. 88-96.
- Fargione G, Gerarci A, La Rosa G, Risitano, 2002. A. Rapid determination of the fatigue curve by the thermographic method. *International Journal of Fatigue*, Vol. 24, p. 11-19.
- Freire J. L. F., Waugh R. C., Fruehmann, R., Dulieu-Barton J. M., 2015. Using thermoelastic stress analysis to detect damaged and hot spot areas in structural components. *J. Mech. Eng. Autom*, Vol. 5, p. 623-634.
- Guamán A., Castro J. T. P., Vieira R. B., Paiva V. E. L., Freire J. L. F., 2017. "Fatigue Limit Assessment of a Low Carbon Steel using Dixon's Up-And-Down and Infrared Thermography Methods" *International Conference on Advances in Experimental Mechanics 29th - 31st August 2017, University of Sheffield, UK*.
- La Rosa G, Risitano A., 1999. Thermographic methodology for the rapid determination of the fatigue limit of materials and mechanical components. *Int J Fatigue Mater Struct Components* 1999; Vol. 22, p. 65-73 [December].
- Nationalbronze <[www.nationalbronze.com/pdfs/C36000.pdf](http://www.nationalbronze.com/pdfs/C36000.pdf)> 2017. (last accessed 29.09).
- Nóbrega M. J. R., 2010. "Influência da metodologia de medição das propriedades mecânicas dinâmicas na previsibilidade do comportamento de estruturas sujeitas a impactos elastoplásticos" *PhD Thesis*, Pontificia Universidade Católica do Rio de Janeiro, Departamento de Engenharia Mecânica.
- Vieira R. B., 2016. "Thermography applied to the study of fatigue in polycarbonate", *MSc. Thesis*, Pontificia Universidade Católica do Rio de Janeiro, Departamento de Engenharia Mecânica.

## 7. RESPONSIBILITY NOTICE

The authors are the only responsible for the printed material included in this paper.

## APPENDIX B -

Macrography and Micrography tests made by photomechanical laboratory

For the presented Brass:

### Test - A: Macrography

ASTM E 3 - 01 – “Standard Guide for Preparation of Metallographic Specimens”.

ASTM E 340-00 -“Standard Test Method for Macroetching Metals and Alloys”.

ASTM A 407-1987- Macroetching Metal and Alloys

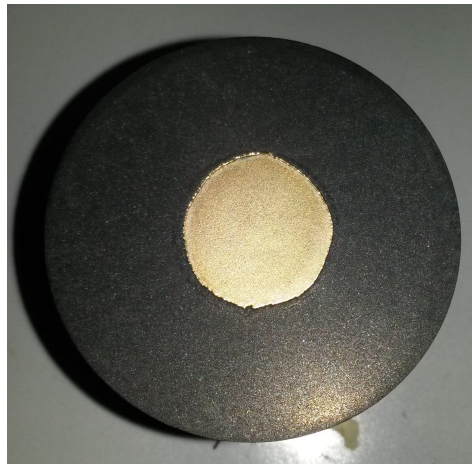


Image 1: Position: Transverse / Attack: Nitric acid / Note: Structure with no apparent deformation.

### Test - B: Micrography

ASTM E 3 - 01 – “Standard Guide for Preparation of Metallographic Specimens”.

ASTM A 384-1987- Microetching Metal and Alloys.

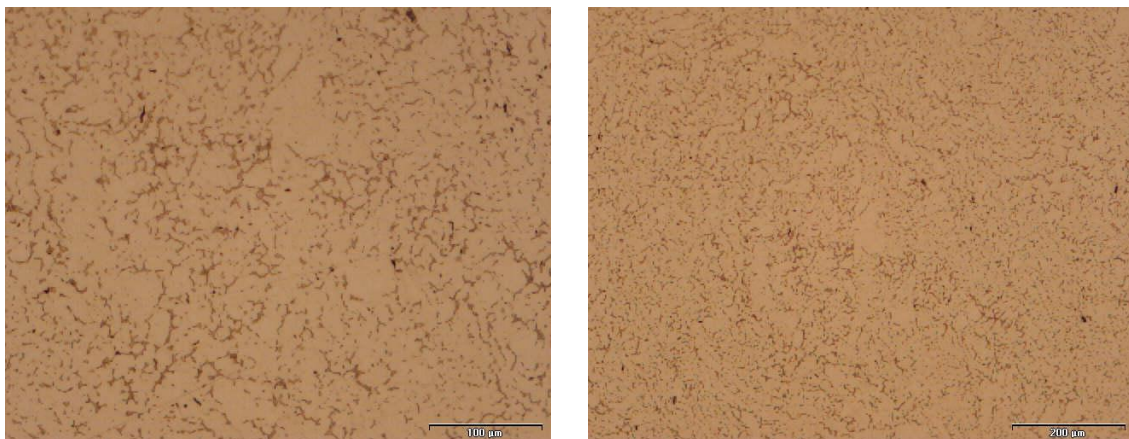


Image 2; 3: Position: Transverse / Attack: Reagent composed of 20g of  $\text{FeCl}_3 \cdot 6 \text{H}_2\text{O}$ , 60 ml of HCl (37%) and 250 ml of ethanol (96%). / Remark: Matrix solution phase  $\alpha$  with phase  $\beta$  / Increase: 100X and 200X.

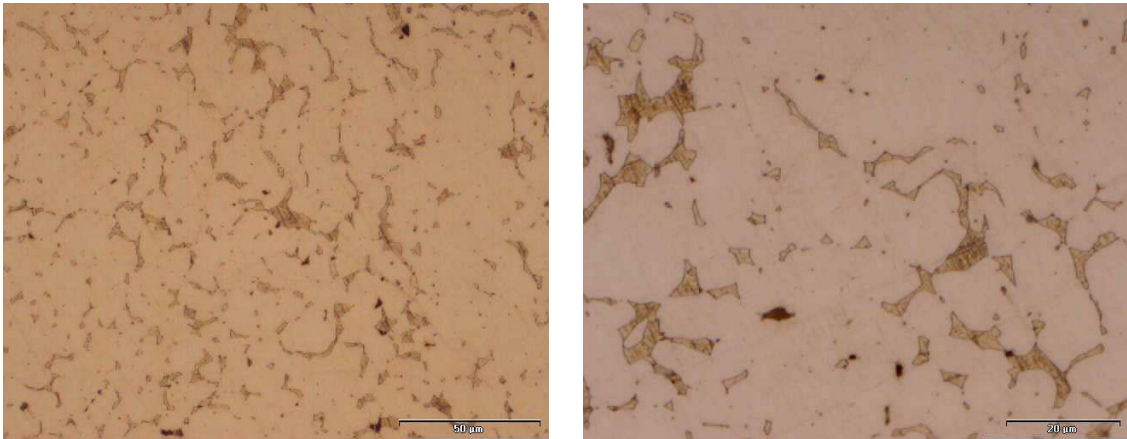


Image 4; 5: Position: Transverse / Attack: Reagent composed of 20g of  $\text{FeCl}_3 \cdot 6 \text{H}_2\text{O}$ , 60 ml of  $\text{HCl}$  (37%) and 250 ml of ethanol (96%). / Remark: Matrix solution phase  $\alpha$  with phase  $\beta$  Minor secretions of Pb and Fe/ Increase: 500X and 1000X.

## Results

It deals with micrographic structure that has characteristics of copper, zinc and lead alloy (Cu-Zn-Pb). In the brass that the Pb amount is up to 3% (content is 0.3 to 3.0%) the Zn content is higher than 35% then a microstructural characteristic and a biphasic alloy ( $\alpha + \beta$ ). Pb affects deformation, so they are alloys in the manufacture of bolts and parts machined from bars and extruded profiles. On the other hand, however, it is not a security service, but there is no contract to guarantee interdisciplinary voids in the solidification improving the tightness.

Note: These alloys are not used for cold plastic deformation processes.

## APPENDIX C -

Macrography and Micrography tests made by photomechanical laboratory

For the presented Aluminium:

### Test - A: Macrography

ASTM E 3 - 01 – “Standard Guide for Preparation of Metallographic Specimens”.

ASTM E 340-00 -“Standard Test Method for Macroetching Metals and Alloys”.

ASTM A 407-1987- Macroetching Metal and Alloys



Image 1: Position: Transverse / Attack: Keller / Note: From the center to peripheral grains equiaxial then columnar grains.

### Test - B: Micrography

ASTM E 3 - 01 – “Standard Guide for Preparation of Metallographic Specimens”.

ASTM A 384-1987- Microetching Metal and Alloys.

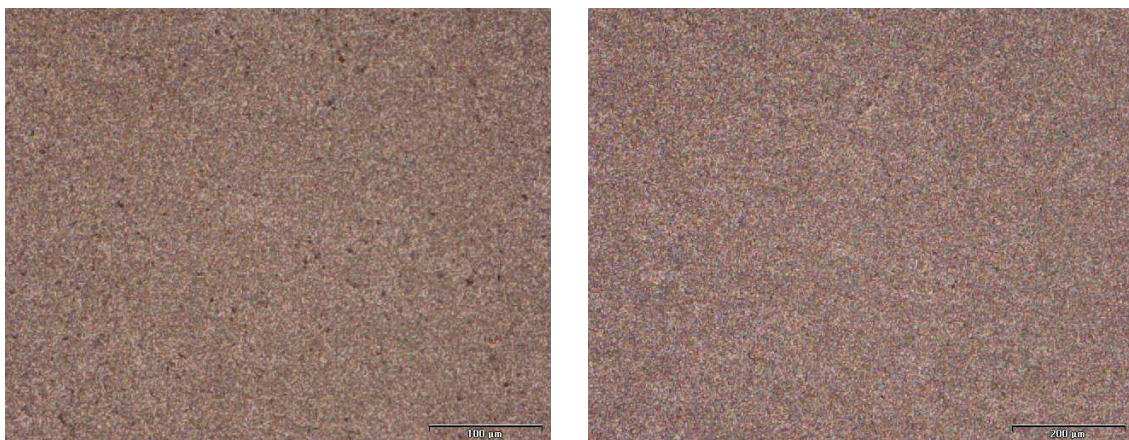


Image 2; 3: Position: Transverse / Attack: Keller / Note: Solid solution matrix  $\alpha$  with dispersed or coagulated precipitates of  $\text{FeAl}_3$ ,  $\text{AlFeSi}$  / Increase: 100X and 200X

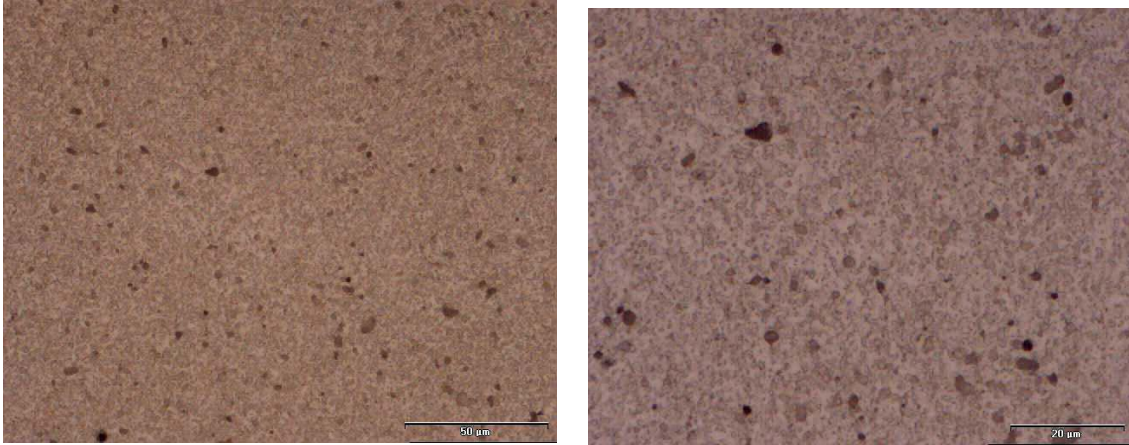


Image 4; 5: Position: Transverse / Attack: Keller / Note: Solid solution matrix  $\alpha$  with dispersed or coagulated precipitates of  $\text{FeAl}_3$ ,  $\text{AlFeSi}$  / Increase: 500X and 1000X

## Results

It is an aluminum alloy that has macrographic characteristics of an extruded or chilled alloy.

The micrographic aspect is of an alloy that has characteristics of normalized material with dispersoids distributed in its texture.